CHIN. PHYS. LETT. Vol. 37, No. 8 (2020) 087104 **Express Letter**

Predicting the Potential Performance in P-Type SnS Crystals via Utilizing the Weighted Mobility and Quality Factor

Wenke He(何文科), Bingchao Qin(秦炳超), and Li-Dong Zhao(赵立东)*

School of Materials Science and Engineering, Beihang University, Beijing 100191, China

(Received 24 June 2020; accepted 7 July 2020; published online 12 July 2020)

The figure of merit ZT is the direct embodiment of thermoelectric performance for a given material. However, as an indicator of performance improvement, the only ZT value is not good enough to identify its outstanding inherent properties, which are highly sought in thermoelectric community. Here, we utilize one powerful parameter to reveal the outstanding properties of a given material. The weighted mobility is used to estimate the carrier transports of p-type SnS crystals, including the differences in doping level, carrier scattering and electronic band structure. We analyze the difference in carrier scattering mechanism for different crystal forms with the same doping level, then evaluate and confirm the temperature-dependent evolution of electronic band structures in SnS. Finally, we calculate the quality factor B based on the weighted mobility, and establish the relationship between ZT and B to further predict the potential performance in p-type SnS crystals with low cost and earth abundance, which can be realized through taking advantage of the inherent material property, thus improving B factor to achieve optimal thermoelectric level.

PACS: 71.20.−b, 72.20.Pa, 84.60.Rb DOI: 10.1088/0256-307X/37/8/087104

Introduction.—The urgent demands for stable, eco-friendly and renewable energy are stimulating the innovation and development of energy utilization technology. Thermoelectric technology is capable of converting heat into electricity from waste heat recovery directly, and has received increasing attention over the past decades.[1−6] In the meanwhile, the exploitation and research of thermoelectric materials are moving forward to high effectiveness, low cost, nontoxicity and environmental protection.[7,8] Generally, the thermoelectric performance for a given material is determined by the figure of merit $ZT = S^2\sigma T/\kappa$, where S, σ, T and κ are the Seebeck coefficient, electrical conductivity, absolute temperature in Kelvin and thermal conductivity (sum of lattice thermal conductivity $\kappa_{\rm lat}$ and electronic thermal conductivity $\kappa_{\rm ele}$), respectively. Since the discovery of tin selenide (SnSe) crystals with potential performance,[9−12] tin sulfide (SnS) as an analogue chalcogenide has come into the sight of researchers gradually.[13,14] SnS is crystallized in the structure with lower symmetry at room temperature (*Pnma* phase), a typical distortion of NaCl-type structure, and it undergoes a displacive-type structure transition to higher symmetric orthorhombic *Cmcm* phase at high temperature.[15] The low lattice thermal conductivity $\kappa_{\rm lat}$ in SnS is intimately associated to its asymmetric crystal structure, mainly arising from the weak bonding character and strong anharmonicity.[16−21] Furthermore, the relevant theoretical calculation results show one surprisingly complex electronic band structure in this simple compound.[17,22−24,25] Therefore, SnS has been considered as a competitive candidate owing to the certain attractive carriers and phonons transports, as well as its abundant reserves and environmental compatibility.

To date, extensive attempts have been conducted to improve the thermoelectric performance of SnS through chemical doping,[14,26−28] Sn vacancy modulation,[29] electronic band structure engineering,[17,25,30] etc. Among these attempts, most of which are aiming at the promotion of electrical transport properties due to the low thermal conductivity in SnS. Owing to the large band gap ($\sim$ 1.2 eV), SnS possesses poor electrical conductivity.[17] Through effective heterovalent doping, however, the carrier concentration can be optimized to the order of $\sim 10^{19}\,{\rm cm}^{-3}$.[17,25,26] Furthermore, the carrier mobility can reach a significant increment by utilizing its high in-plane carrier mobility in the form of crystals compared to the polycrystalline SnS.[17,25] The simultaneous enhancement of both carrier concentration and carrier mobility, to the maximum extent, gives rise to the increase of electrical conductivity. In addition, the multi-band transports caused by the improved carrier concentration benefits from the complex elec-

Supported by the National Key Research and Development Program of China (Grant Nos. 2018YFA0702100 and 2018YFB0703600), the National Natural Science Foundation of China (Grant Nos. 51632005 and 51772012), the Beijing Natural Science Foundation (Grant No. JQ18004), the Shenzhen Peacock Plan Team (Grant No. KQTD2016022619565991), 111 Project (Grant No. B17002), and the National Science Fund for Distinguished Young Scholars (Grant No. 51925101).

*Corresponding author. Email: zhaolidong@buaa.edu.cn

© 2020 Chinese Physical Society and IOP Publishing Ltd

tronic band structure essentially, which results in a huge enhancement of Seebeck coefficient.[17,28] However, it is not clear whether the performance improvement is from an enhancement of the inherent material property or the optimization of carrier concentration. Therefore, it is of great importance to analyze the carrier transport mechanism for understanding of the electrical properties in SnS.

The weighted mobility ($\mu_{\rm w}$), a type of mobility weighted by the density of electronic states, provides an alternative way to assess the carriers transport characteristics without the aid of band structure calculations.[31] The weighted mobility can help to estimate the differences in doping level, carrier scattering mechanism and electronic band structure.[32,33] The weighted mobility estimation conducted in SnSe crystals indicated the performance improvement originates from the doubled effective mass via carrier concentration optimization, revealing the significant contribution of complex valence bands in optimizing the final thermoelectric performance.[34] Nevertheless, the inherent material property (e.g., electronic band structure) has not been discussed in-depth. Hence, from this point of view, we want to uncover the material transport nature through the estimation of SnS crystals. In this work, we make comprehensive assessment on the carrier transport characteristics of p-type SnS by the weighted mobility. With optimized doping level, we estimate the difference in scattering mechanism through comparing SnS with crystalline and polycrystalline forms. Then we analyze and confirm the temperature-dependent interaction of three electronic valance bands and the evolution promoted by Se alloying in SnS crystals, which facilitates the electrical transport properties. Finally, we conduct the relationship of ZT values with reduced electron chemical potential (η) and quality factor B, and predict the maximum ZT ($ZT_{\rm max}$) with B factor through utilizing optimized η of p-type SnS.

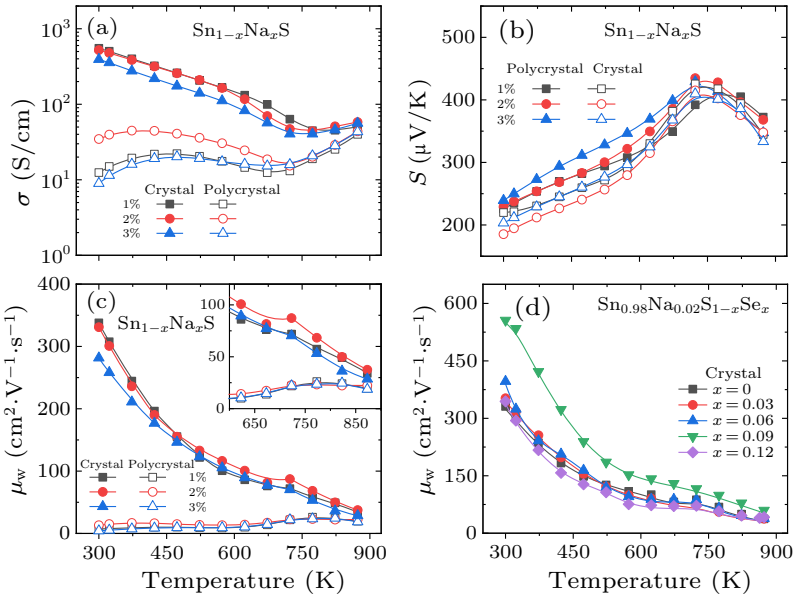

Fig. 1. Electrical transport properties as a function of temperature for SnS-based crystals and polycrystals. (a) Electrical conductivity for $Sn_{1-x}Na_xS$. (b) Seebeck coefficient for $Sn_{1-x}Na_xS$. (c) Weighted mobility for $Sn_{1-x}Na_xS$, inset shows the enlarged temperature range at 600–900 K. (d) Weighted mobility for $Sn_{0.98}Na_{0.02}S_{1-x}Se_x$ crystals. The thermoelectric performance of SnS crystals are plotted for comparison.[17,30]

Analysis of the scattering mechanism.—The weighted mobility can be calculated using experimental Seebeck coefficient and electrical conductivity, which is a convenient and effective method to evaluate the carrier transport behaviors. We have synthesized polycrystalline SnS samples with Na doping to compare with that of crystals,[17] so as to analyze the difference in carrier transports in SnS with different crystal forms, respectively. The carrier concentrations of these samples are optimized to the level of $\sim 10^{19}\,{\rm cm}^{-3}$. Compared with the SnS crystals, the electrical conductivity of polycrystalline SnS is more than one order of magnitude lower especially at room temperature [Fig. 1(a)]. According to the Drude-Sommerfeld free electron model $\sigma = ne\mu$ (where σ is the electrical conductivity, n the carrier concentration, e the electronic charge and μ the carrier mobility), the high electrical conductivity in SnS crystals mainly

comes from the improved carrier mobility due to the elimination of grain boundary. The temperature dependence of Seebeck coefficients for all SnS samples are almost in the same level [Fig. 1(b)], indicating that the electronic band structure was slightly affected by the crystal forms at the same doping level. On the basis of experimental electrical conductivity and Seebeck coefficient, the weighted mobility can be calculated easily, as shown in Fig. 1(c). The weighted mobility in SnS crystals is apparently superior to the polycrystalline samples in the entire temperature range, which demonstrates that the existence of grain boundary brings about strong carrier scattering. The weighted mobility in SnS crystals decreases with temperature as $\sim T^{-3/2}$, indicating that the carriers are predominately scattered by acoustic phonons.[35] However, the weighted mobility in polycrystalline SnS is extremely low, especially at high temperatures, which implies more complex scattering behaviors based on grain boundary, such as grain size,[31] lattice disorder,[36] or ionized impurity scattering[37] in polycrystalline samples. Given the complexity and uncertainty of scattering mechanism over the entire temperature range in polycrystalline SnS, it is intractable to analyze the carrier transport behavior with temperature. Therefore, crystal-form SnS is perfect enough to estimate the carrier transports with temperature for p-type SnS due to the complete removal of grain boundary resistance.

In our previous work, we found the temperature-dependent interplay of three electronic valance bands and this behavior was promoted after Se alloying in SnS crystals.[30] Furthermore, we calculated the weighted mobility for all the samples with Se alloying to assess the electronic band structure, as shown in Fig. 1(d). It can be seen that the weighted mobility approximatively follows a relationship of $\sim T^{-3/2}$, demonstrating a dominated acoustic phonon scattering.[35] In addition, the weighted mobility has been significantly enhanced via 9% Se alloying, which shows a great improvement of electrical transport properties in SnS crystals. The detailed analysis of the electrical transport mechanism related to electronic band structure will be discussed below.

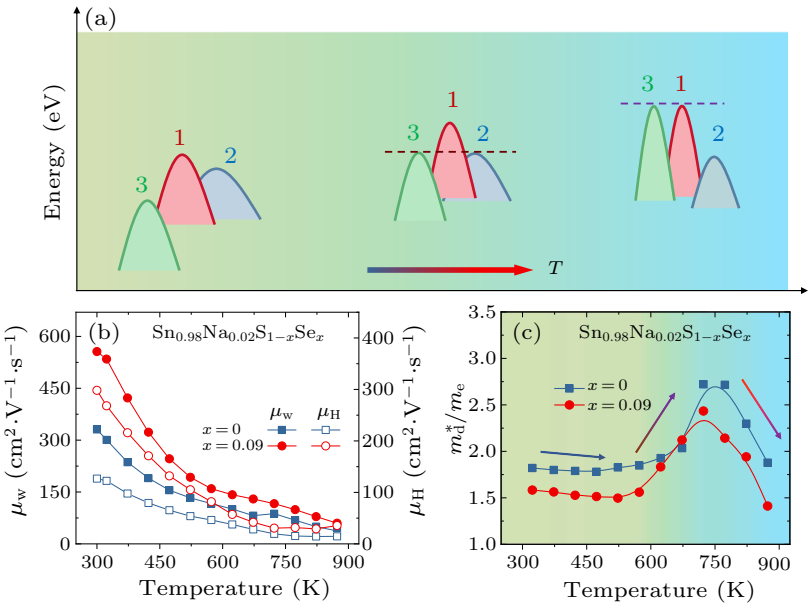

Fig. 2. Temperature-dependent electronic band structure and thermoelectric parameter calculations for $Sn_{0.98}Na_{0.02}S_{1-x}Se_x$ ($x = 0$, 0.09) crystals (Ref. [30]). (a) Schematic evolution of three separate valence bands with rising temperature in SnS. The number "1", "2" and "3" in panel (a) denote "VBM1", "VBM2" and "VBM3", respectively. (b) Weighted mobility and Hall mobility as a function of temperature. (c) The ratio m_d^*/m_e as a function of temperature.

Evaluation of electronic band structure.—The triple band evolution with temperature in SnS crystals is responsible for excellent electrical properties.[30] The schematic diagram in Fig. 2(a) illustrates the dynamic evolution of these three valence bands, marked as the first valence band maximum (VBM1), the second VBM (VBM2) and the third VBM (VBM3). With increasing temperature, VBM1 and VBM2 diverge while VMB3 and VBM1 converge, meanwhile VBM2 and VBM3 experience band convergence before diverging. The electronic band structure involves the effective mass (m^*) of the electronic bands, which could be a good descriptor of the band evolution behavior in SnS, so the analysis of band structure can turn to the m^*. Generally, the weighted mobility μ_w is related to the Hall mobility μ_H expressed as

$\mu_w \approx \mu_H(m_d^*/m_e)^{3/2}$, where m_d^* is the density of states (DOS) effective mass and m_e is the electron mass.[38] The comparison between μ_w and μ_H of SnS crystals is presented in Fig. 2(b), both of them show similar temperature-dependent behaviors. The DOS effective mass m_d^* can be approximatively evaluated through the weighted mobility μ_w divided by Hall mobility μ_H, shown in Fig. 2(c). The variation of m_d^* with temperature can be divided into three stages in SnS. The m_d^* changes a little before ~ 600 K, then increases to the maximum at ~ 750 K and finally declines to the initial value around. This process agrees well with the dynamic evolution of the three separated electronic valance bands, as illustrated in Fig. 2(a). The increase of m_d^* can well explain the band convergence of VBM2 and VBM3, and the reduced m_d^* is related to the divergence from VBM3 (lighter band) rising and VBM2 (heavier band) dropping. Moreover, the m_d^* decreases after Se alloying and the temperature behavior of m_d^* has been promoted in SnS. Therefore, the change in m_d^* could well elucidate and confirm the three-valance-band transports in SnS crystals.

If it is assumed that the m_d^* remains constant in the whole temperature range, that is, there is no fluctuation in the valence bands, we calculated a simulated weighted mobility with fixed m_d^* at 300 K, which is compared with the μ_w above to evaluate the role of band structures with temperature in SnS. As shown in Fig. 3(a), there is an obvious deviation above ~ 600 K, namely, the actual μ_w is higher than the assumed one, which shows that the band evolution is favorable especially in the high-temperature region as it can maintain the high electrical performance. After Se alloying, this superiority becomes more pronounced [inset of Fig. 3(a)]. Therefore, excellent electrical transport properties in SnS are tightly relevant with the electronic band structure, which can be well estimated by the weighted mobility.

The weighted mobility is a good descriptor of the electronic qualities that constitute a good thermoelectric material. In a material with optimized doping level, the ZT value is proportional to the thermoelectric quality factor B, defined as:[31]

$$B = \left(\frac{k_B}{e}\right)^2 \frac{8\pi e\,(2m_e k_B T)^{3/2}}{3h^3} \cdot \frac{\mu_w}{\kappa_{lat}} T, \qquad (1)$$

where k_B, h and e represent Boltzmann's constant, Planck constant and electronic charge, respectively. From Eq. (1), the B factor is proportional to the weighted mobility divided by lattice thermal conductivity μ_w/κ_{lat}. Thus, the assessment of thermoelectric performance optimization mainly focuses on μ_w/κ_{lat}. Based on the thermoelectric transport properties,[30] we calculate the temperature dependence of μ_w/κ_{lat} for SnS samples as shown in Fig. 3(b). After 9% Se alloying, the values of μ_w/κ_{lat} are obviously higher than that of Se-free SnS. Certainly, the high values come from not only the improved μ_w but also from the reduced κ_{lat} via Se alloying. Furthermore, the B factors of these two samples are also calculated for comparison. As shown in the inset of Fig. 3(b), the B factor after Se alloying can reach ~ 1.2 at 873 K, which is twice as large as the Se-free one. Therefore, B is a good indicator of whether the thermoelectric performance of a given material is optimized. We will further establish the relationship between B factor and ZT as follows.

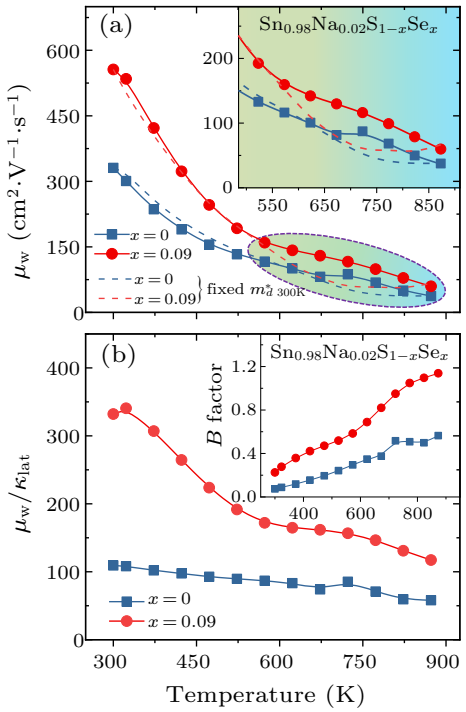

Fig. 3. Weighted mobility and its ratio to lattice thermal conductivity as a function of temperature for $Sn_{0.98}Na_{0.02}S_{1-x}Se_x$ ($x = 0$, 0.09) crystals (Ref. [30]). (a) Weighted mobility and corresponding simulated mobility (dotted line) with the effective mass fixed at 300 K, and the inset shows great deviation at high temperature range. (b) The ratio μ_w/κ_{lat} as a function of temperature, and the inset shows the temperature dependence of quality factor B.

Analysis of quality factor and ZT value.—The quality factor approach can consider ZT as a function of two independent variables: the reduced Fermi level (reduced electron chemical potential) $\eta = E_F/k_BT$ and B factor.[39] The former is a function of doping and temperature, which can be extracted from the Seebeck coefficient. On the other hand, σ_E is a transport coefficient with units of conductivity that characterizes the capability of material conducts electricity for a given η, which can be derived from Seebeck coefficient S and electrical conductivity σ. Thus, σ_E as a function of S and σ can be expressed below, where η is the parameter:

$$\sigma = \sigma_E \cdot \ln(1 + e^{\eta}), \qquad (2)$$

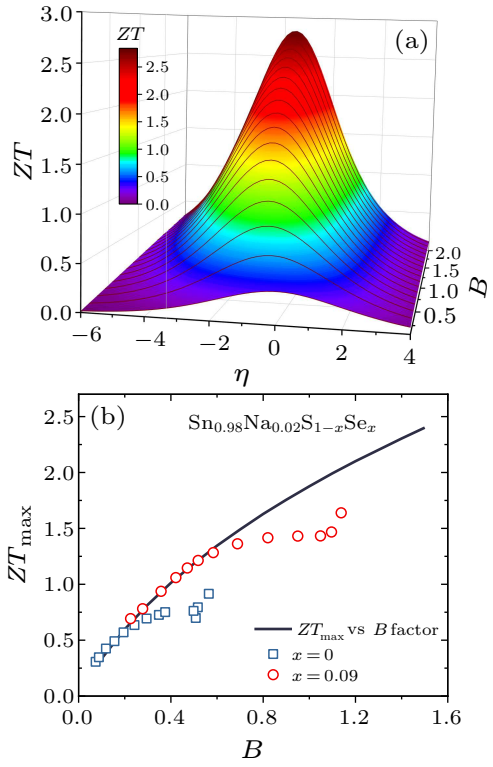

Fig. 4. The ZT values as a function of the reduced Fermi level η and quality factor B. (a) The ZT values as a function of η and B. (b) The maximum ZT values with optimized η as a function of B factor. The corresponding ZT values of $Sn_{0.98}Na_{0.02}S_{1-x}Se_x$ ($x = 0$, 0.09) crystals with B factor are plotted for comparison (Ref. [30]).

when the $|S|$ is large ($|S| > 120\,\mu V/K$ within 5%),

$$\sigma_E = \sigma \cdot \exp\left(\frac{|S|}{k_B/e} - 2\right). \tag{3}$$

Combined with Eqs. (2) and (3), the $|S(\eta)|$ as an indicator of η can be derived. Besides, the Lorenz number L, determined by electronic thermal conductivity $\kappa_{ele} = L\sigma T$, is also as a function of η by using the measurements of $|S|$ at given temperature, defined as:

$$L[10^{-8}W \cdot \Omega/K^2] \approx 1.5 + \exp\left(-\frac{|S|}{116\mu V/K}\right). \tag{4}$$

The other independent variable B factor can also be express as:[40]

$$B = \left(\frac{k_B}{e}\right)^2 \frac{\sigma_E}{\kappa_{lat}} T. \tag{5}$$

Therefore, the ZT can be written as:

$$ZT = \frac{S^2\sigma T}{\kappa_{lat} + \kappa_{ele}} = \frac{S^2}{\frac{\kappa_{lat}}{\sigma T} + L} = \frac{S^2(\eta)}{\frac{\kappa_{lat}}{\sigma_E \ln(1+e^{\eta})T} + L(\eta)}$$
$$= \frac{S^2(\eta)}{\frac{(k_B/e)^2}{B\ln(1+e^{\eta})} + L(\eta)}. \tag{6}$$

From Eq. (6), the ZT as a function of these two independent parameters (η and B) is plotted in Fig. 4(a). With increasing B factor, the ZT value versus η curve rises up. The maximum ZT (ZT_{max}) with different B factor can be achieved through optimizing carrier concentration (thus the η). The B factor determines the optimum level of a material property although it is independent of carrier concentration. In addition, the B factor can also well estimate the achievable ZT_{max} when the carrier concentration is optimized. Hence, we extract ZT_{max} from optimized η under different B factor and plot the curve ZT_{max} versus B factor [Fig. 4(b)]. The ZT_{max} shows positive correlation to the B factor. The corresponding ZT values under different temperatures in SnS samples extracted from Fig. 3(b) are also plotted for comparison in Fig. 4(b). Compared with the Se-free SnS, the B factor is higher and the ZT values are closer to the ZT_{max} curve after Se alloying, which can well explain the synergetic optimization effects in SnS with Se alloying. Moreover, the ZT values are deviated from the optimal curve at higher B factor (thus higher temperature) in SnS, which indicates the further potential improvement at higher temperatures through boosting B factor under optimized η.

Conclusion and outlooks.—In summary, the weighted mobility can well describe the inherent carrier transports of a material. Through evaluating the weighted mobility for p-type SnS, the difference in scattering mechanism with different crystal forms can be distinguished, and the temperature-dependent evolution of electronic band structure can be evaluated. Based on the weighted mobility, the quality factor B can be derived to estimate the thermoelectric quality for the materials with an optimized doping level. Moreover, the ZT_{max} can be used to assess the optimal level of a material through the establishment between ZT value and quality factor B, which could give reasonable prediction of potential performance for p-type SnS crystals. The B factor improvement in SnS, to a large extent, shows the superiority of this material's inherent properties. Therefore, the further thermoelectric performance promotion in the low-cost SnS crystals can be realized by utilizing the inherent features thus improving B factor, such as synergistic optimization of complex electronic band structure, electron-phonon modulation, etc.

References

[1] He J and Tritt T M 2017 *Science* **357** eaak9997
[2] Snyder G J and Toberer E S 2008 *Nat. Mater.* **7** 105
[3] Zhang X and Zhao L D 2015 *J. Materiomics* **1** 92
[4] Qin B C, Xiao Y, Zhou Y M and Zhao L D 2018 *Rare Met.* **37** 343
[5] Gao L, Liu Q L, Yang J W, Wu Y, Liu Z H, Qin S J, Ye X B, Jin S F, Li G D, Zhao H Z and Long Y W 2020 *Chin. Phys. Lett.* **37** 066202
[6] Zhou K, Zhang T, Liu B and Yao Y J 2020 *Chin. Phys. Lett.* **37** 017102

[7] Wei T R, Wu C F, Li F and Li J F 2018 *J. Materiomics* **4** 304
[8] Xiao Y and Zhao L D 2020 *Science* **367** 1196
[9] Zhao L D, Lo S H, Zhang Y, Sun H, Tan G, Uher C, Wolverton C, Dravid V P and Kanatzidis M G 2014 *Nature* **508** 373
[10] Zhou Y and Zhao L D 2017 *Adv. Mater.* **29** 1702676
[11] Shang P P, Dong J, Pei J, Sun F H, Pan Y, Tang H, Zhang B P, Zhao L D and Li J F 2019 *Research* **2019** 1
[12] Zhou L Y, Zheng Q, Bao L H and Liang W J 2020 *Chin. Phys. Lett.* **37** 017301
[13] Tan Q and Li J F 2014 *J. Electron. Mater.* **43** 2435
[14] Tan Q, Zhao L D, Li J F, Wu C F, Wei T R, Xing Z B and Kanatzidis M G 2014 *J. Mater. Chem. A* **2** 17302
[15] Chattopadhyay T, Pannetier J and Von Schnering H G 1986 *J. Phys. Chem. Solids* **47** 879
[16] Shafique A and Shin Y H 2017 *Sci. Rep.* **7** 10
[17] He W, Wang D, Dong J F, Qiu Y, Fu L, Feng Y, Hao Y J, Wang G T, Wang J F, Liu C, Li J F, He J Q and Zhao L D 2018 *J. Mater. Chem. A* **6** 10048
[18] Zhao L D, Chang C, Tan G and Kanatzidis M G 2016 *Energy & Environ. Sci.* **9** 3044
[19] Qu W W, Zhang X X, Yuan B F and Zhao L D 2018 *Rare Met.* **37** 79
[20] Chang C and Zhao L D 2018 *Mater. Today Phys.* **4** 50
[21] Feng B, Li G Q, Hu X M, Liu P H, Li R S, Zhang Y L, Li Y W, He Z and Fan X A 2020 *Chin. Phys. Lett.* **37** 037201
[22] Volykhov A A, Shtanov V I and Yashina L V 2008 *Inorg. Mater.* **44** 345
[23] Parker D and Singh D J 2010 *J. Appl. Phys.* **108** 083712
[24] Hao S, Dravid V P, Kanatzidis M G and Wolverton C 2016 *APL Mater.* **4** 104505
[25] Wu H, Lu X, Wang G, Peng K, Chi H, Zhang B, Chen Y, Li C, Yan Y, Guo L, Uher C, Zhou X and Han X 2018 *Adv. Energy Mater.* **8** 1800087
[26] Zhou B, Li S, Li W, Li J, Zhang X, Lin S, Chen Z and Pei Y 2017 *ACS Appl. Mater. & Interfaces* **9** 34033
[27] Tang H, Dong J F, Sun F H, Asfandiyar, Shang P and Li J F 2019 *Sci. Chin. Mater.* **62** 7
[28] Wang Z, Wang D, Qiu Y, He J and Zhao L D 2019 *J. Alloys Compd.* **789** 485
[29] Yang H Q, Wang X Y, Wu H, Zhang B, Xie D D, Chen Y J, Lu X, Han X D, Miao L and Zhou X Y 2019 *J. Mater. Chem. C* **7** 3351
[30] He W, Wang D, Wu H *et al.* 2019 *Science* **365** 1418
[31] Snyder G J, Snyder A H, Wood M, Gurunathan R, Snyder B H and Niu C 2020 *Adv. Mater.* **32** 2001537
[32] Imasato K, Fu C, Pan Y, Wood M, Kuo J J, Felser C and Snyder G J 2020 *Adv. Mater.* **32** 1908218
[33] Slade T J, Grovogui J A, Kuo J J, Anand S, Bailey T P, Wood M, Uher C, Snyder G J, Dravid V P and Kanatzidis M G 2020 *Energy & Environ. Sci.* **13** 1509
[34] Qin B, He W and Zhao L D 2020 *J. Materiomics* DOI:10.1016/j.jmat.2020.06.003
[35] May A F, Toberer E S, Saramat A and Snyder G J 2009 *Phys. Rev. B* **80** 125205
[36] Xie H H, Wang H, Fu C, Liu Y, Snyder G J, Zhao X and Zhu T 2015 *Sci. Rep.* **4** 6888
[37] Mao J, Shuai J, Song S *et al.* 2017 *Proc. Natl. Acad. Sci. USA* **114** 10548
[38] May A F and Snyder G J 2017 *Materials, Preparation, and Characterization in Thermoelectrics* (CRC press) p. 11
[39] Kang S D and Snyder G J 2017 arXiv:1710.06896 [cond-mat.mtrl-sci]
[40] Kang S D and Snyder G J 2017 *Nat. Mater.* **16** 252